

A Study on Quality of 12-Pulse Rectifier Source Feeding Three-Level T-NPC Inverter Under Switch-Open-Circuit Fault SVPWM Control

Nguyen Hong Phong Le¹, Dang Khoa Pham¹, Tan Luong Van², Duc Hieu Nguyen³,
Van Nho Nguyen^{1*}

¹Ho Chi Minh City University of Technology (HCMUT), VNU-HCM, Vietnam

²Ho Chi Minh City University of Industry and Trade, Vietnam

³Tra Vinh University, Vietnam

*Corresponding author. Email: nvnho@hcmut.edu.vn

ARTICLE INFO

Received: 19/01/2025
Revised: 25/03/2025
Accepted: 20/06/2025
Published online: 31/10/2025

KEYWORDS

Common-mode voltage;
Switch-open-circuit;
Three-level t-type neutral-point-clamped inverter;
Twelve-pulse rectifier;
Phase-shifting transformer;
Fault-tolerant control.

ABSTRACT

This paper studies the quality of a 12-pulse diode rectifier source feeding a three-level T-NPC inverter working under a space vector PWM control for switch-open-circuit fault, denoted as SVPWM2. Before the occurrence of the aforementioned fault, the inverter was working under conventional reduced common-mode voltage space vector PWM algorithm, denoted as SVPWM1 and providing the output voltage for a three-phase R-L load. The input and output currents of phase-shifting transformer, the input power factor of transformer, and the capacitor voltages at the DC-link are investigated. Simulation results show that the SVPWM2 method has the same characteristics as pre-fault space vector method (SVPWM1) in terms of total harmonic distortion of transformer primary and secondary currents, as well as input power factor. However, SVPWM2 has higher deviation in capacitor voltage compared to SVPWM1. Regarding to power losses, SVPWM2 has higher switching loss yet lower conduction loss than those of SVPWM1. The overall efficiency of SVPWM2 is slightly higher compared to that of SVPWM1.

Doi: <https://doi.org/10.54644/jte.2025.1791>

Copyright © JTE. This is an open access article distributed under the terms and conditions of the [Creative Commons Attribution-NonCommercial 4.0 International License](https://creativecommons.org/licenses/by-nc/4.0/) which permits unrestricted use, distribution, and reproduction in any medium for non-commercial purpose, provided the original work is properly cited.

1. Introduction

Three-level (3L) T-type neutral-point-clamped (T-NPC) voltage source inverter (VSI) has several advantages compared to traditional two-level VSI (2L VSI) and 3L NPC VSI [1], [2]. The 3L T-NPC inverter is preferred to be used in high-power photovoltaic (PV) systems and low-voltage variable speed drives (VSD) [3].

Pulse-width modulation (PWM) schemes present a popular technique for controlling VSIs to made high performance and flexible output control. However, PWM techniques generate common-mode voltage (CMV). CMV is the main source of several problems in VSI-based systems, for example, causing bearing currents, which can damage the structure and lubricants of bearings part in electric machines [1], or leading to EMI noise and the deterioration of the stator insulation [1]. In order to reduce CMV for a 3L T-NPC VSI, there are a huge number of research works proposed earlier, which can be divided into two types: hardware-based solutions [4] and software-based solutions [1], [5]. Software-based solutions are preferred due to their simplicity and economic benefits. The main principle of this type of technique is to use switching vectors which CMV magnitude are zero or one-sixth of DC-link voltage [5].

The 3L T-NPC VSI has several issues regarding the reliability of operating [2], [6], [7]. For a semiconductor power switch, two typical failures can occur: switch-short-circuit (SSC) fault and switch-open-circuit (SOC) fault, respectively [8], [9]. For safety reasons, the inverter normally stops working under SSC fault [7], [10]. Another fault named SOC fault occurs due to malfunction of gate driver circuits or the lifting of bonding wire caused by thermal cycling [8], [9], [10]. This kind of fault will lead to the deterioration of system performances, for instance, the distortion of output voltages and

Table 1. Switching states and output voltages of 3L T-NPC VSI, $X = \{A, B, C\}$

| S_{X1} | S_{X2} | S_{X3} | S_{X4} | $S_X = S_{X1} + S_{X2}$ | $v_{XO} = S_X(V_d/2)$ | $v_{XG} = v_{XO} - V_d/2 = (S_X - 1).(V_d/2)$ |
|----------|----------|----------|----------|-------------------------|-----------------------|---|
| 0 | 0 | 1 | 1 | 0 | 0 | $-V_d/2$ |
| 0 | 1 | 1 | 0 | 1 | $V_d/2$ | 0 |
| 1 | 1 | 0 | 0 | 2 | V_d | $V_d/2$ |

Referring to Figure 1, the instantaneous value of common-mode voltage, v_{cm} , can be determined by:

$$v_{cm} = v_{NG} = (v_{AG} + v_{BG} + v_{CG})/3 \quad (1)$$

With the relationship that $v_{XG} = (S_X - 1).(V_d/2)$ with $X = \{A, B, C\}$, equation (1) becomes:

$$v_{cm} = \frac{1}{3}(S_A + S_B + S_C - 3)\frac{V_d}{2} \quad (2)$$

From (2), in order to limitation the CMV magnitude between $-V_d/6 \leq v_{cm} \leq +V_d/6$, the value of $(S_A + S_B + S_C)$ must be 2, 3, or 4. The space vectors satisfy this condition are shown in the space vector diagram (SVD) in Figure 2(a). The traditional RCMV space vector PWM technique, denoted as SVPWM1, can be implemented by using nearest-three-vector (NTV) and DPWM principles.

However, under SOC fault in S_{A2}/S_{A3} , the switching state of $S_A = 1$ can not be generated. Under this situation, there are only two available values of S_A , i.e. $S_A = 0$ and $S_A = 2$. The switching states of phase B and phase C are not affected by this SOC fault. Therefore, the calculation of S_B and S_C in SVPWM2 are as the same as those in SVPWM1. The number of RCMV space vectors are now reduced from 19 to 12, as shown in Figure 2(b).

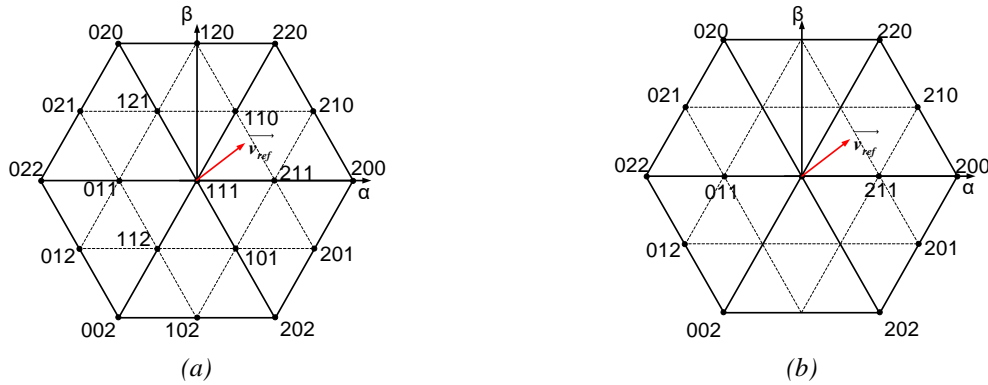


Figure 2. RCMV space vector diagram of 3L T-NPC inverter:

a) In normal operation (SVPWM1), b) In SOC fault occurred in one T-switch of phase A

2.2. SOC fault control SVPWM (SVPWM2)

2.2.1. Region determination

From the SVD in Figure 2(b), in order to develop the fault-tolerant control SVPWM technique, denoted as SVPWM2, the regions on space vector diagram (SVD) are re-determined. The principles for region determination are nearest-three-vector (NTV) and discontinuous PWM (DPWM). The SVD is now divided into 24 regions, as shown in Figure 3. For example, in the first quadrant of the SVD, region 1 is determined by the NTVs $\{211, 210, 220\}$ while for region 2, the set of $\{210, 220, 020\}$ is selected. For region 6, there are two available candidate sets, i.e. $\{210, 020, 021\}$ and $\{210, 220, 021\}$. The set $\{210, 220, 021\}$ is selected because two vectors 210 and 220 are nearer to region 6 than two vectors 020 and 021.

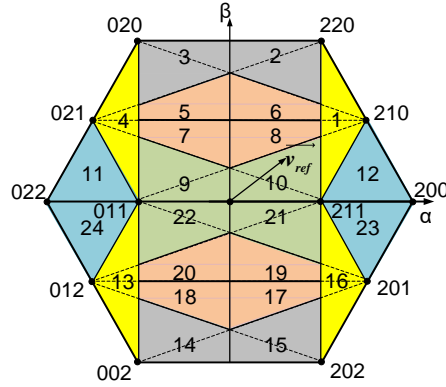


Figure 3. Proposed regions in SVPWM2.

2.2.2. Dwelling time calculation

Region 10 is chosen as an example for calculating dwelling time. The formula to synthesize \vec{v}_{ref} is as follows:

$$\begin{cases} \vec{v}_{ref} = d_1 \vec{v}_1 + d_2 \vec{v}_2 + d_3 \vec{v}_3 \\ d_1 + d_2 + d_3 = 1 \end{cases} \quad (3)$$

where d_1 , d_2 , and d_3 are the dwelling factors corresponding to \vec{v}_1 , \vec{v}_2 , and \vec{v}_3 , respectively, and $0 \leq d_1, d_2, d_3 \leq 1$. The values of each vector are $\vec{v}_1 = (1/2 + j\sqrt{3}/6)$, $\vec{v}_2 = 1/3$ and $\vec{v}_3 = -1/3$, respectively. Solving (3) in α - β coordinates leading to the following results:

$$d_1 = d_{210} = 2A, d_2 = d_{211} = -5A + B + 1 / 2, d_3 = d_{011} = A - B + 1 / 2 \quad (4)$$

in which $A = m \cdot \sin \theta$ and $B = m \sqrt{3} \cdot \cos \theta$. The value $m = \sqrt{3} V_{ref} / V_d$ is the modulation index. For this study, the maximum value of m is 1.

2.2.3. Space vector implementation

Table 2 lists the nearest-three vector (NTV) selection, the duty factors, and pulse patterns for the proposed algorithm for all 24 regions.

Table 2. Space vector implementation of SVPWM2

| Region | NTV selection | Duty factors | Pulse pattern |
|--------|---------------|---|---------------------|
| 1 | 211, 210, 220 | $d_{211} = -A - B + 2, d_{210} = 2B - 2, d_{220} = A - B + 1$ | 211-210-220-210-211 |
| 2 | 210, 220, 020 | $d_{210} = -2A + 2, d_{220} = (5A + B - 4)/2, d_{020} = (-A - B + 2)/2$ | 210-220-020-220-210 |
| 3 | 021, 020, 220 | $d_{021} = -2A + 2, d_{020} = (5A - B - 4)/2, d_{220} = (-A + B + 2)/2$ | 021-020-220-020-021 |
| 4 | 011, 021, 020 | $d_{011} = -A + B + 2, d_{021} = -2B - 2, d_{020} = A + B + 1$ | 011-021-020-021-011 |
| 5 | 021, 020, 210 | $d_{021} = (-5A - B + 4)/3, d_{020} = 2A - 1, d_{210} = (-A + B + 2)/3$ | 021-020-210-020-021 |
| 6 | 210, 220, 021 | $d_{210} = (-5A + B + 4)/3, d_{220} = 2A - 1, d_{021} = (-A - B + 2)/3$ | 210-220-021-220-210 |
| 7 | 021, 011, 210 | $d_{021} = (5A - B - 1)/3, d_{011} = -2A + 1, d_{210} = (A + B + 1)/3$ | 021-011-210-011-021 |
| 8 | 210, 211, 021 | $d_{210} = (5A + B - 1)/3, d_{211} = -2A + 1, d_{021} = (A - B + 1)/3$ | 210-211-021-211-210 |

| | | | |
|----|---------------|---|---------------------|
| 9 | 021, 011, 211 | $d_{021} = 2A, d_{011} = (-5A - B + 1)/2, d_{211} = (A + B + 1)/2$ | 021-011-211-011-021 |
| 10 | 210, 211, 011 | $d_{210} = 2A, d_{211} = (-5A + B + 1)/2, d_{011} = (A - B + 1)/2$ | 210-211-011-211-210 |
| 11 | 011, 021, 022 | $d_{011} = -A + B + 2, d_{021} = 2A, d_{022} = -A - B - 1$ | 011-021-022-021-011 |
| 12 | 211, 210, 200 | $d_{211} = -A - B + 2, d_{210} = 2A, d_{200} = -A + B - 1$ | 211-210-200-210-211 |
| 13 | 011, 012, 002 | $d_{011} = A + B + 2, d_{012} = -2B - 2, d_{002} = -A + B + 1$ | 011-012-002-012-011 |
| 14 | 012, 002, 202 | $d_{012} = 2A + 2, d_{002} = (-5A - B - 4)/2, d_{202} = (A + B + 2)/2$ | 012-002-202-002-012 |
| 15 | 201, 202, 002 | $d_{201} = 2A + 2, d_{202} = (-5A + B - 4)/2, d_{002} = (A - B + 2)/2$ | 201-202-002-202-201 |
| 16 | 211, 201, 202 | $d_{211} = A - B + 2, d_{201} = 2B - 2, d_{202} = -A - B + 1$ | 211-201-202-201-211 |
| 17 | 201, 202, 012 | $d_{201} = (5A + B + 4)/3, d_{202} = -2A - 1, d_{012} = (A - B + 2)/3$ | 201-202-012-202-201 |
| 18 | 012, 002, 201 | $d_{012} = (5A - B + 4)/3, d_{002} = -2A - 1, d_{201} = (A + B + 2)/3$ | 012-002-201-002-012 |
| 19 | 201, 211, 012 | $d_{201} = (-5A + B - 1)/3, d_{211} = 2A + 1, d_{012} = (-A - B + 1)/3$ | 201-211-012-211-201 |
| 20 | 012, 011, 201 | $d_{012} = (-5A - B - 1)/3, d_{011} = 2A + 1, d_{201} = (-A + B + 1)/3$ | 012-011-201-011-012 |
| 21 | 201, 211, 011 | $d_{201} = -2A, d_{211} = (5A + B + 1)/2, d_{011} = (-A - B + 1)/2$ | 201-211-011-211-201 |
| 22 | 012, 011, 211 | $d_{012} = -2A, d_{011} = (5A - B + 1)/2, d_{211} = (-A + B + 1)/2$ | 012-011-211-011-012 |
| 23 | 211, 201, 200 | $d_{211} = A - B + 2, d_{201} = -2A, d_{200} = A + B - 1$ | 211-201-200-201-211 |
| 24 | 011, 012, 022 | $d_{011} = A + B + 2, d_{012} = -2A, d_{022} = A - B - 1$ | 011-012-022-012-011 |

The block diagram for implementation SVPWM2 is shown in Figure 4.

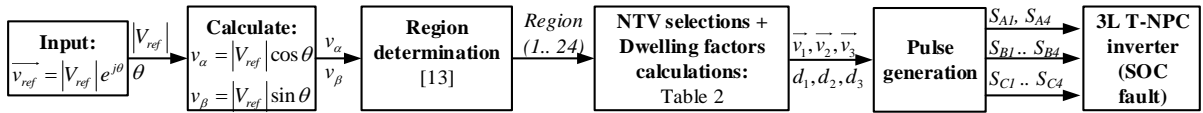


Figure 4. Control structure of the T-NPC inverter system

3. Simulation Results

A MATLAB/Simulink model was built to simulate the system in Figure 1. Simulation parameters are listed in Table 3.

Table 3. Simulation parameters

| Parameter | Notation | Value | Unit |
|---|------------|-----------------------|------|
| Grid voltage (line voltage) | V_g | 400 | V |
| Transformer rated apparent power | S_B | 10000 | VA |
| Transformer secondary wye-winding voltage | V_2 | 230 | V |
| Transformer secondary delta-winding voltage | V_3 | 230 | V |
| Rated DC-link voltage | V_d | 600 | V |
| DC-link capacitances | C_1, C_2 | 2000×10^{-6} | F |
| Fundamental output frequency | f | 50 | Hz |
| Switching frequency | f_{sw} | 5000 | Hz |

| | | | |
|-----------------|---|-------|----------|
| Load resistance | R | 16 | Ω |
| Load inductance | L | 0.050 | H |

3.1. Simulation results for PST

Figure 5 shows the waveforms of primary current (i_{pri_A}), secondary wye-winding current (i_{secw_A}), and secondary delta-winding current (i_{secd_A}) of the PST corresponding to $m = 0.4$ and $m = 0.9$. The spectra of these current are shown in Figure 6 ($m = 0.4$) and in Figure 7 ($m = 0.9$), respectively.

The spectra of i_{pri_A} in Figure 6(a) and Figure 7(a) do not have 5th and 7th harmonic components, and the 17th and 19th components are inconsiderable. By contrast, the spectra of i_{secw_A} and i_{secd_A} have these odd harmonic components, i.e. 5th, 7th, 11th and 13th harmonic order.

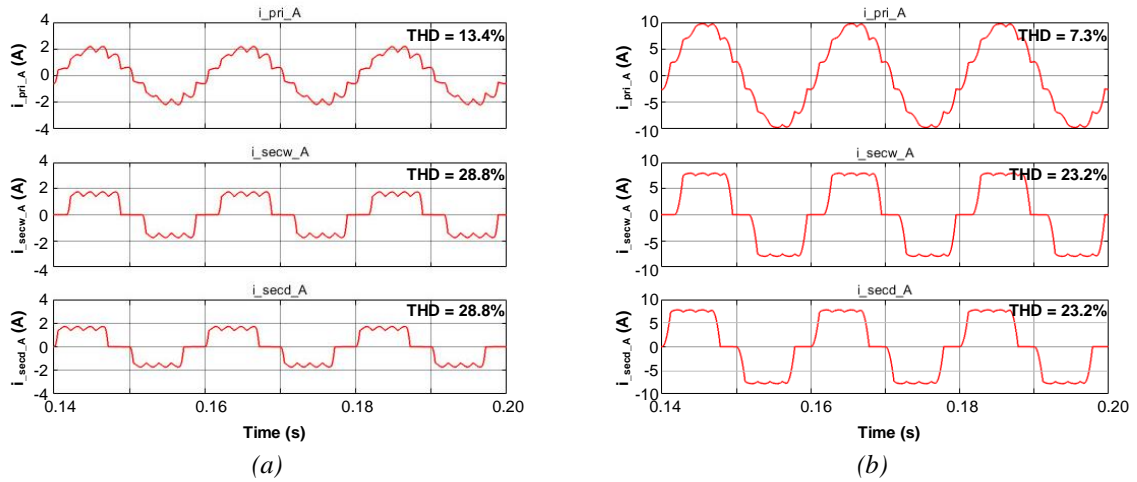


Figure 5. Waveforms of PST currents:

a) m = 0.4, and b) m = 0.9 ($f_{maxFFT} = 2.5$ kHz). From top to bottom: i_{pri_A} , i_{secw_A} , and i_{secd_A} .

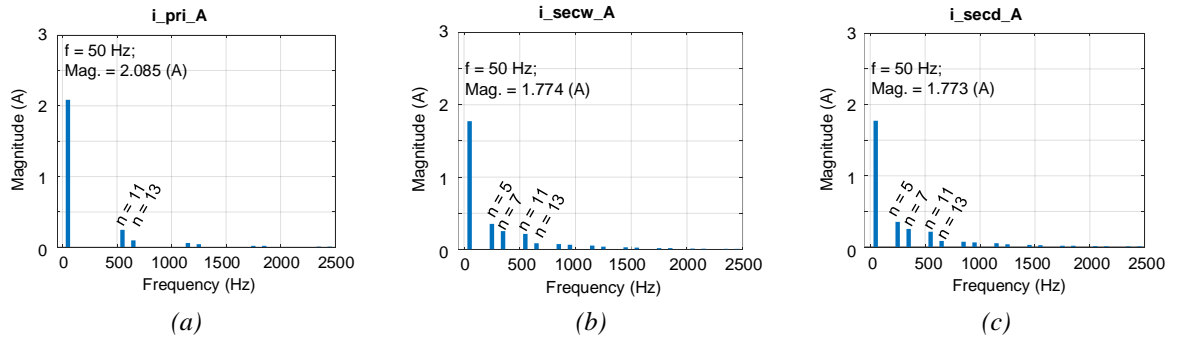


Figure 6. Spectra of PST currents with $m = 0.4$: *a) i_{pri_A} , (b) i_{secw_A} , and c) i_{secd_A} ($f_{maxFFT} = 2.5$ kHz).*

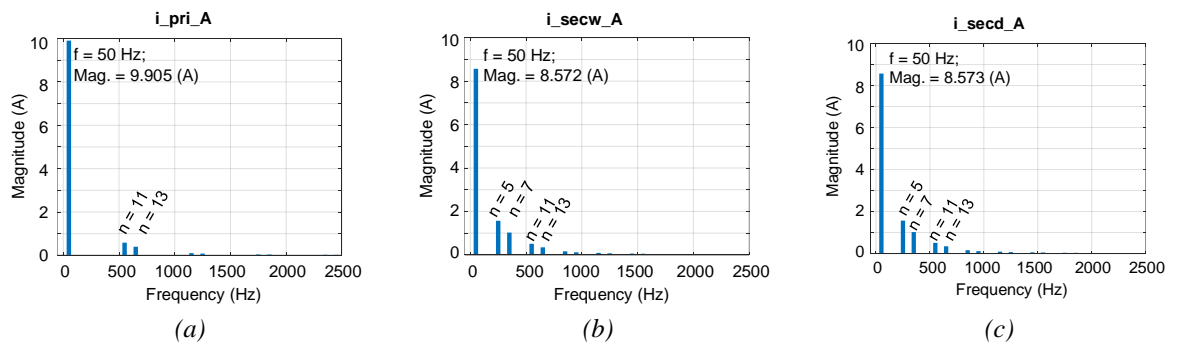


Figure 7. Spectra of PST currents with $m = 0.9$: *a) i_{pri_A} , (b) i_{secw_A} , and c) i_{secd_A} ($f_{maxFFT} = 2.5$ kHz).*

The THD characteristics of i_{pri_A} is shown in Figure 8(a), and primary side power factor (PF_{pri}) is shown in Figure 8(b). For comparison purpose, characteristics of SVPWM2 are presented along with those of SVPWM1, which is the SVPWM method for controlling the inverter before the occurrence of SOC fault. From Figure 8, SVPWM2 has the same characteristics compared to SVPWM1. With $m > 0.6$, $THD(i_{pri_A})$ is less than 10%. The transformer has high input power factors ($PF_{pri} > 0.97$) in the whole range of modulation index.

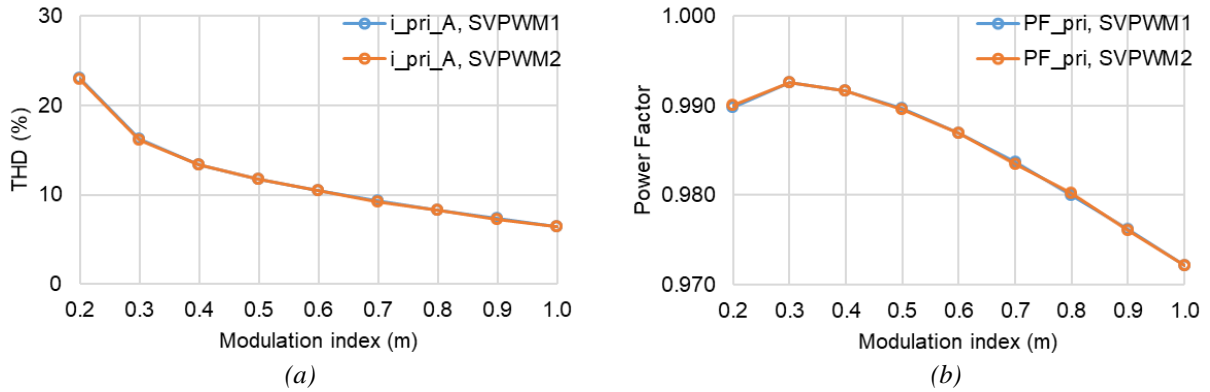


Figure 8. PST primary side characteristics versus modulation index (m):

a) THD of i_{pri_A} ($f_{maxFFT} = 2.5$ kHz), and b) Input PF (PF_{pri}).

Regarding to THD characteristics of secondary currents (i_{secw_A} and i_{secd_A}), from Figure 9 it is seen that the SVPWM2 also has the same behavior as SVPWM1 in the whole range of m . THD characteristics of i_{secw_A} and i_{secd_A} are identical.

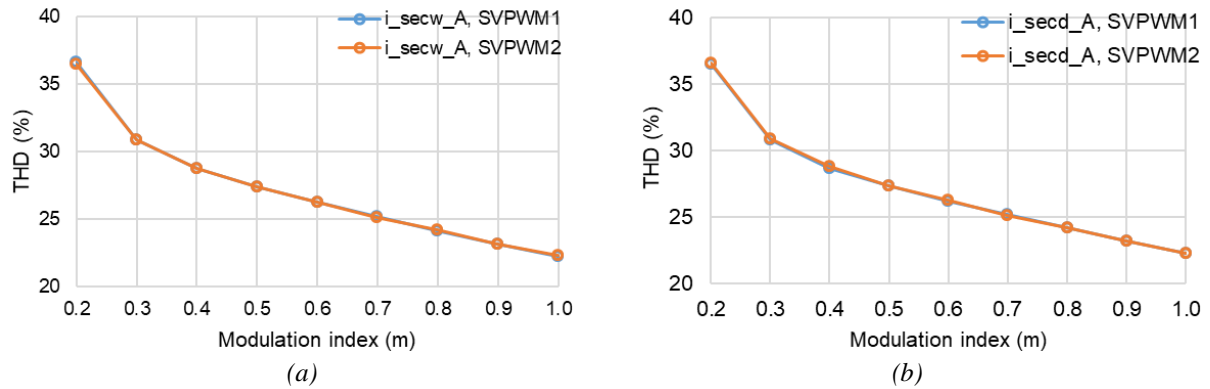


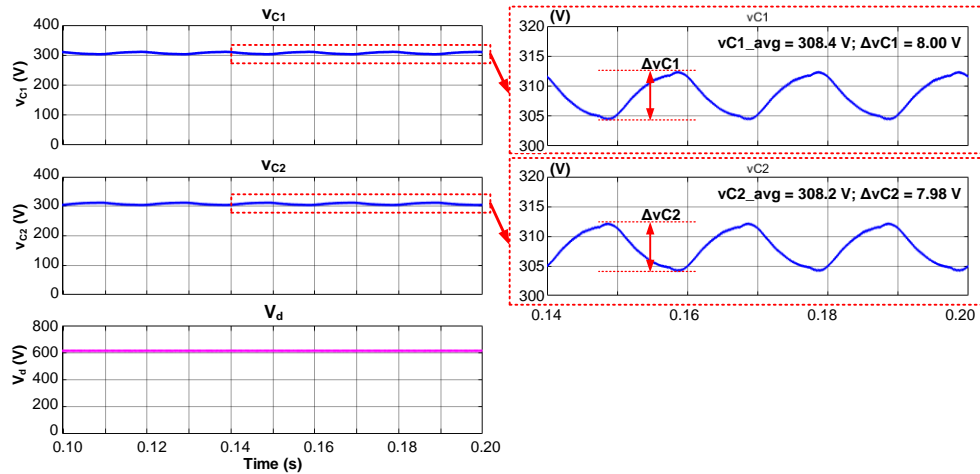
Figure 9. PST secondary current THD characteristics versus modulation index (m):

a) i_{secw_A} , and b) i_{secd_A} ($f_{maxFFT} = 2.5$ kHz).

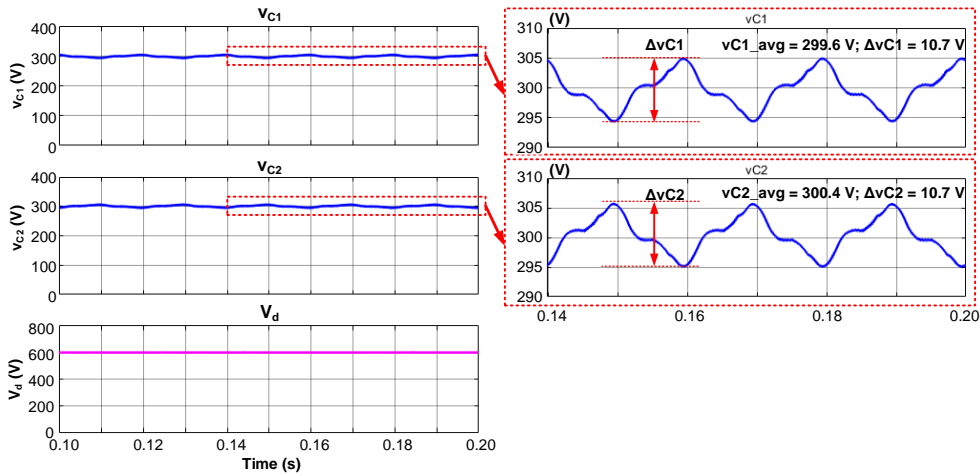
3.2. Simulation results for DC-link capacitors

The waveforms of capacitor voltages and DC-link voltage in SVPWM2 are shown in Figure 10. Each capacitor shares a half of DC-link voltage. At low modulation index ($m = 0.4$), the average voltage on each capacitor is slightly higher than rated value: $v_{C1_avg} = 308.4$ V and $v_{C2_avg} = 308.2$ V, and the voltage ripple on each capacitor is about 8 V. For high value of m ($m = 0.9$), the voltage ripple increase to 10.7 V. At $m = 0.9$, each capacitor has the voltage as rated value, i.e. 300 V.

The characteristics of capacitor voltage ripple are shown in Figure 11. Overall, all ripples are lower than 4%. The SVPWM2 has higher ripple compared to SVPWM1 which is about 2 times for $m > 0.7$. For example, at $m = 0.9$, Δv_{C1} and Δv_{C2} in SVPWM2 are 3.6% while those in SVPWM1 are 1.7%.



(a)



(b)

Figure 10. DC-link voltage waveforms for SVPWM2:

a) $m = 0.4$, b) $m = 0.9$. From top to bottom: C1 voltage (v_{C1}), C2 voltage (v_{C2}), and total DC-link voltage (V_d).

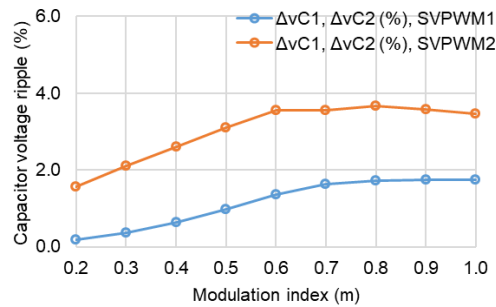


Figure 11. Voltage ripple characteristics of DC-link capacitors (Δv_{C1} , Δv_{C2} normalized to rated V_{C1} and V_{C2}) versus modulation index (m).

3.3. Simulation results for loss evaluation

A PLECS simulation model was built in order to calculate power losses. Figure 12 shows the switching loss and conduction loss of SVPWM2 compared to SVPWM1. The efficiency characteristics are presented in Figure 13. From Figure 12(a), SVPWM2 has higher switching loss than SVPWM1, especially at low modulation index ($m < 0.7$). However, the conduction loss of SVPWM2 is lower than that of SVPWM1, as shown in Figure 12(b). Overall, the efficiency of SVPWM2 is slightly higher than SVPWM1, as shown in Figure 13.

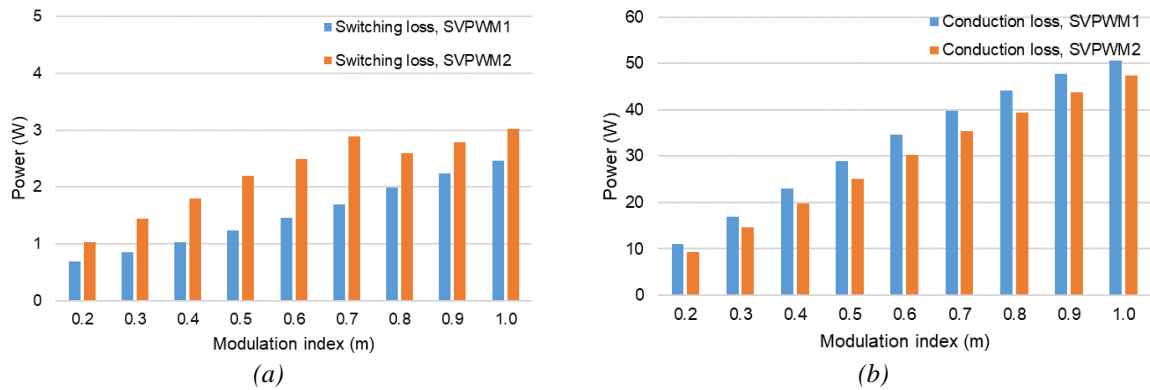


Figure 12. Power losses of SVPWM2 and SVPWM1 versus modulation index: a) Switching loss, and b) Conduction loss

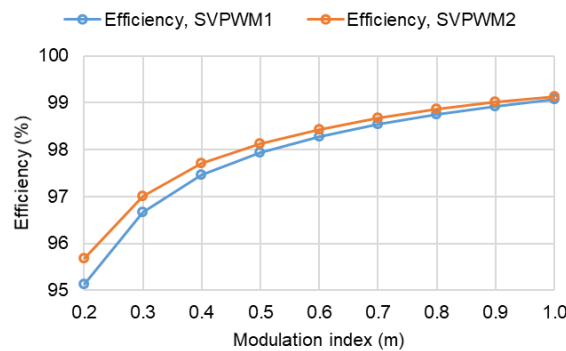


Figure 13. Efficiency of SVPWM2 and SVPWM1 versus modulation index.

4. Conclusion

This paper presents the quality of a 12-pulse rectifier feeding a 3L T-NPC VSI working under SVPWM control for SOC fault. The transformer currents and capacitor voltages are measured and analyzed in different values of the inverter modulation indices. Simulation results show that SVPWM2 has the same characteristics as SVPWM1 in terms of transformer input and output currents, and transformer input power factor for the whole range of modulation indices. However, SVPWM2 has higher capacitor voltage ripples compared to SVPWM1. Compared to previously proposed methods for controlling the T-NPC inverter under SOC fault, SVPWM2 is more economic due to the fact that this method does not require any additional hardware. In addition, based on the re-design of SVPWM control, the output voltage of the inverter could be as high as pre-fault SVPWM1.

The potential avenues for future research are as follows:

- 1) Implementing SVPWM2 using carrier-based PWM (CBPWM) principle. This type of PWM method is simple in calculation and implementation compared to SVPWM.
- 2) Developing a RCMV model predictive control (MPC) algorithm for controlling the inverter under SOC fault. MPC is a popular method used recent years for power electronics converters. Due to the number of RCMV vectors is reduced from 19 (in SVPWM1) to 12 (in SOC fault), the computation burden of this method can also be reduced.

Acknowledgement

The authors acknowledge the University of Technology (HCMUT), VNU-HCM, for supporting this study.

Conflict of interests

The authors declare that there is no conflict of interests regarding the publication of this paper.

Table of abbreviations

| Abbreviations | Definition |
|---------------|--------------------------------------|
| CMV | Common-Mode Voltage |
| DPWM | Discontinuous Pulse-Width Modulation |
| ESPWM | Eight-Switch Pulse-Width Modulation |
| ESTPI | Eight-Switch Three-Phase Inverter |
| NPC | Neutral-Point-Clamped |
| NTV | Nearest-Three-Vector |
| PST | Phase-Shifting Transformer |
| PWM | Pulse-Width Modulation |
| RCMV | Reduced Common-Mode Voltage |
| SOC | Switch-Open-Circuit |
| SSC | Switch-Short-Circuit |
| SVD | Space Vector Diagram |
| SVPWM | Space Vector Pulse-Width Modulation |
| THD | Total Harmonic Distortion |
| T-NPC | T-Type Neutral-Point-Clamped |
| VSD | Variable Speed Drives |
| VSI | Voltage Source Inverter |


REFERENCES

- [1] E. Robles, M. Fernandez, J. Zaragoza, I. Aretxabaleta, I. M. De Alegria, and J. Andreu, "Common-Mode Voltage Elimination in Multilevel Power Inverter-Based Motor Drive Applications," in *IEEE Access*, vol. 10, pp. 2117-2139, 2022.
- [2] U. Choi, K. Lee, and F. Blaabjerg, "Diagnosis and Tolerant Strategy of an Open-Switch Fault for T-Type Three-Level Inverter Systems," in *IEEE Trans. Ind. Appl.*, vol. 50, no. 1, pp. 495-508, 2014.
- [3] S. Cailhol, P. Vidal, and F. Rotella, "A Generic Method of Pulse width Modulation Applied to Three-Phase Three-Level T-Type NPC Inverter," in *IEEE Trans. Ind. Appl.*, vol. 54, no. 5, pp. 4515-4522, 2018.
- [4] A. Hota, S. Jain, and V. Agarwal, "A Modified T-Structured Three-Level Inverter Configuration Optimized With Respect to PWM Strategy Used for Common-Mode Voltage Elimination," in *IEEE Trans. Ind. Appl.*, vol. 53, no. 5, pp. 4779-4787, 2017.
- [5] W. Zhu, D. D. Gaetano, X. Chen, G. W. Jewell, and Y. Hu, "A Review of Modeling and Mitigation Techniques for Bearing Currents in Electrical Machines With Variable-Frequency Drives," in *IEEE Access*, vol. 10, pp. 125279-125297, 2022.
- [6] B. Wang, Z. Li, Z. Bai, P. T. Krein, and H. Ma, "A Redundant Unit to Form T-Type Three-Level Inverters Tolerant of IGBT Open-Circuit Faults in Multiple Legs," in *IEEE Trans. Power Electron.*, vol. 35, no. 1, pp. 924-939, Jan. 2020.
- [7] J. Wang, W. Zhang, W. Jiang, M. Ma, Q. Zhang, and X. Huang, "Application Ranges of Fault-Tolerant Control for T-Type Three-Level Inverter Under Single/Multi-phase Open-Circuit Faults of Inner Switches," in *IEEE Access*, vol. 8, pp. 207599-207609, 2020.
- [8] S. Xu, J. Zhang, and J. Hang, "Investigation of a Fault-Tolerant Three-Level T-Type Inverter System," in *IEEE Trans. Ind. Appl.*, vol. 53, no. 5, pp. 4613-4623, 2017.
- [9] J. He, R. Katchbi, N. Weise, N. A. O. Demerdash, and L. Wei, "A Fault-Tolerant T-Type Multilevel Inverter Topology With Increased Overload Capability and Soft-Switching Characteristics," in *IEEE Trans. Ind. Appl.*, vol. 53, no. 3, pp. 2826-2839, 2017.
- [10] T. Lee, B. Li, M. Yang, and Y. Tsai, "A Carrier-Based PWM for Three-Level T-Type Inverter to Tolerate Open-Circuit Fault," in *IEEE Trans. Power Electron.*, vol. 33, no. 10, pp. 8787-8796, Oct. 2018.
- [11] U. M. Choi, F. Blaabjerg, and K. B. Lee, "Reliability Improvement of a T-Type Three-Level Inverter With Fault-Tolerant Control Strategy," in *IEEE Trans. Power Electron.*, vol. 30, no. 5, pp. 2660-2673, May 2015.
- [12] J. Chen, C. Zhang, A. Chen, and X. Xing, "Fault-Tolerant Control Strategies for T-Type Three-Level Inverters Considering Neutral-Point Voltage Oscillations," in *IEEE Trans. Ind. Electron.*, vol. 66, no. 4, pp. 2837-2846, April 2019.
- [13] H. P. N. Le, K. D. Pham, and N. V. Nguyen, "Analyses, Modeling, and SVPWM Control of a Three-Level T-NPC Inverter to Reduce Common-Mode Voltage Under Open-Circuit Fault in a Neutral-Point Switch," in *IEEE Access*, vol. 12, pp. 104708-104727, 2024.

Nguyen Hong Phong Le received the B.S. degree from Industrial University of Ho Chi Minh City, Vietnam, in 2012, and the M.S. degree from University of Technology, Vietnam National University Ho Chi Minh City (HCMUT-VNU), Vietnam, in 2018, respectively, both in Electrical Engineering. He is currently pursuing the Ph.D. degree in Electrical Engineering at HCMUT-VNU, Vietnam. His research interests include modeling and control of power electronics converters and pulse-width modulation techniques for multilevel inverters.

Email: lnhphong.sdh221@hcmut.edu.vn. ORCID:  <https://orcid.org/0009-0000-0992-9412>

Dang Khoa Pham was born in Ho Chi Minh City, Vietnam in 1990. He received his B.S and M.S. degrees in Electrical Engineering from the Ho Chi Minh University of Technology, Ho Chi Minh City, Vietnam, where he is presently working towards his Ph.D. degree in Electrical Engineering. His current research interest includes AC motor control, renewable energy, and PWM converters.

Email: khoadangpham@hcmut.edu.vn. ORCID:  <https://orcid.org/0000-0003-3875-285X>

Tan Luong Van received the B.S and M.S degrees in electrical engineering from Ho Chi Minh City University of Technology, Ho Chi Minh city, Vietnam, in 2003 and 2005, respectively, and Ph.D degree in electrical engineering from Yeungnam University, Gyeongsan, South Korea in 2013. Currently, he has been a Faculty Member in the Dept. of Electrical and Electronic Engineering, Ho Chi Minh City University of Industry and Trade, Ho Chi Minh City, Viet Nam. His research interests include power converters, dc/dc converters, machine drives, wind power generation, power quality and power system.

Email: luongvt@huit.edu.vn. ORCID:  <https://orcid.org/0000-0002-8151-3785>

Duc Hieu Nguyen is currently with Tra Vinh University, Tra Vinh, Vietnam as a lecturer. His research interests include electrical machines, power electronics and automation control in industry.

Email: ndhieu@tvu.edu.vn. ORCID:  <https://orcid.org/0009-0002-0141-7695>

Van Nho Nguyen (Member, IEEE) was born in Vietnam in 1964. He received the M.S. and Ph.D. degrees in electrical engineering from the University of West Bohemia, Plzen, Czech Republic, in 1988 and 1991, respectively. Since 1992, he has been with the Department of Electrical and Electronics Engineering, Ho Chi Minh City University of Technology, Ho Chi Minh City, Vietnam, where he is currently an Associate Professor. He was with the Korea Advanced Institute of Science and Technology as a Postdoctoral Fellow for six months in 2001 and a Visiting Professor for one year in 2003-2004. His research interests include modeling and control of switching power active filters, and pulse width modulation techniques for power converters.

Email: nvnho@hcmut.edu.vn. ORCID:  <https://orcid.org/0000-0002-0181-5469>